Ray-trace modeling of acoustic Green's function based on the semiclassical (eikonal) approximation

Rok Prislan[a)]
Department of Physics, Faculty of Mathematics and Physics, University of Ljubljana, Jadranska 19, SI-1000 Ljubljana, Slovenia

Gregor Veble
School of Applied Sciences, University of Nova Gorica, Vipavska 13, SI-5000 Nova Gorica, Slovenia

Daniel Svenšek
Department of Physics, Faculty of Mathematics and Physics, University of Ljubljana, Jadranska 19, SI-1000 Ljubljana, Slovenia

(Received 2 May 2016; revised 4 August 2016; accepted 8 September 2016; published online 17 October 2016)

The Green's function (GF) for the scalar wave equation is numerically constructed by an advanced geometric ray-tracing method based on the eikonal approximation related to the semiclassical propagator. The underlying theory is first briefly introduced, and then it is applied to acoustics and implemented in a ray-tracing-type numerical simulation. The so constructed numerical method is systematically used to calculate the sound field in a rectangular (cuboid) room, yielding also the acoustic modes of the room. The simulated GF is rigorously compared to its analytic approximation. Good agreement is found, which proves the devised numerical approach potentially useful also for low frequency acoustic modeling, which is in practice not covered by geometrical methods. [http://dx.doi.org/10.1121/1.4964295]

[MV] Pages: 2695–2702

I. INTRODUCTION

State-of-the-art sound field modeling in the complete audible frequency range requires separate treatment of low and high frequencies. In the low frequency range, wave-based methods such as boundary element methods (BEM),[1] finite element methods (FEM),[2] and finite difference methods (FDM)[3] are best suited. Although they use different mathematical and methodological approaches that have their advantages and disadvantages for specific types of problems, they all solve the complete wave equation for a given geometry and boundary conditions. As such, wave methods include all properties of waves—interference, diffraction, and scattering—which significantly shape the low-frequency sound field. The efficiency of wave methods is limited to low frequencies. They operate on a discrete grid of points/elements in space (also referred to as the mesh), and to achieve results with acceptable accuracy several points per wavelength are needed. This requirement makes the wave methods convenient as long as the wavelength is not much smaller than the size of the computational domain, i.e., the size of the investigated room. At higher frequencies, wave methods become over demanding in terms of processing time and memory usage.[4,5]

Therefore, geometrical methods are used at higher frequencies. These methods are well established and broadly used in applied acoustics,[6] e.g., in commercial room acoustics simulation engines such as ODEON[7] and CATT-Acoustic.[8] It has been demonstrated that they can be used also in semi-confined geometries, i.e., for outdoor sound propagation modeling (see, e.g., Refs. 9 and 10). Generally, there exist many various implementations of geometrical methods, which however all reside on two basic approaches: (1) the ray-tracing method,[6] which stochastically models the propagation of sound energy, and (2) the image source method,[11] which geometrically constructs virtual sound sources. Both approaches have been ramified in various forms (e.g., beam tracing[12]) and have also been implemented in hybrid casts combining advantages of each.[13] For a review of the state-of-the-art geometrical techniques, cf., e.g., Refs. 14–16.

Notwithstanding their diverse implementations, most of the geometrical methods deal exclusively with the energy of sound waves. There do exist image source implementations that include also the phase information.[13,17–20] To our knowledge, only that of Ref. 20 has been tested below the *Schröder frequency*[21] (not including the lowest eigenmodes, though), however, with a focus other than a rigorous reproduction of individually resolved resonances.

The current study presents a possible direction toward overcoming the high–low frequency dualism of acoustic modeling. We devise a ray-tracing method based on the Van-Vleck equation, which resides on the semiclassical approximation in quantum mechanics[22] and is closely related to the eikonal approximation[23] of geometrical optics.[24] In this way interference phenomena are captured, which is a prerequisite for extending a method to the lower frequency range relevant to acoustics. Moreover, the potency of the method lies in its capability of directly and within the semiclassical theory mathematically rigorously reproducing the acoustic Green's function (GF) of the room (i.e., fundamental solution of the

[a)]Electronic mail: rok.prislan@gmail.com

wave equation), and it is this rigor in particular, that distinguishes our approach from previous implementations of geometrical modeling methods that have also included the phase information. To the best of our knowledge, the presented method has not been systematically applied to acoustics, although its validity for wave systems in certain types of geometries is known. As we will show, it accurately reproduces the resonance frequencies for the studied geometry type and furthermore furnishes acoustic eigenmodes of the correct shape. Inherent to the semiclassical approximation, like any geometrical method it does not capture diffraction effects. Please note, however, that this is not the only limitation (a lesser one, usually) of geometrical methods, as will be demonstrated once more in this study (cf. also, e.g., Ref. 20).

Let us stress that the primary aim of this first approach is the proof of concept and transfer of theoretical framework invented in other scientific areas to acoustics, rather than a fully applied case study or technical assessment of method's performance, which are steps to follow. In order to facilitate the analysis of the numeric results and make the verification of the method as conclusive as possible, we consider the cleanest possible three-dimensional geometry—a cuboid room with a homogeneous boundary condition (which is, however, of a mixed type and complex, i.e., absorbing). Moreover, the known absence of diffraction in a rectangular geometry enables one to isolate and investigate the accuracy issues of the method that are not connected with diffraction—which is the utmost maneuver space available to geometrical methods.

As relevant for potential realistic applications, the method can also handle more complicated geometries with arbitrary inhomogeneous, absorbing, or/and inertive/reactive boundary conditions that can depend on frequency, angle of incidence, and can, as well, represent diffuse (stochastic) reflection, all of these without compromising the computational efficiency. For the present purpose we implement strictly specular reflections corresponding to the aforementioned absorbing boundary condition.

The article is organized as follows. In Sec. II, the theory of the semiclassical propagator is briefly reviewed and applied to the acoustic case. This section also discusses several crucial aspects of the numerical implementation. In Sec. III, the approximate GF is calculated analytically. The results are presented, compared, and discussed in Sec. IV. Main conclusions are drawn in Sec. V.

II. THEORY

In this section, the theory of the semiclassical propagator is applied to the acoustic case of geometrical sound rays. The relevant concepts and equations are presented and interpreted, without deriving or describing them in detail as this would substantially exceed the scope of the paper. For a more thorough introduction of the underlying physical/mathematical theory, the interested reader should start with Ref. 22 and work his way through the references therein. Furthermore, in this section we also present several crucial aspects that are vital for the numerical implementation, as well as for a full understanding of the obtained results.

The whole concept rests on the analogy between the Schrödinger equation for the probability density amplitude Ψ of a quantum mechanical particle of mass m,

$$-\frac{\hbar^2}{2m}\nabla^2\Psi + V(\mathbf{r})\Psi - \mathrm{i}\hbar\frac{\partial\Psi}{\partial t} = 0, \tag{1}$$

with $V(\mathbf{r})$ the space-dependent potential of the particle and $\hbar$ the reduced Planck constant, and the scalar wave equation for the sound pressure field,

$$-\nabla^2 p + \frac{1}{c^2}\frac{\partial^2 p}{\partial t^2} = 0. \tag{2}$$

In general, the speed of sound c can also vary in space, but the variation must be negligible on the scale of the wavelength λ, $\nabla c/c \ll 1/\lambda$, for the wave equation to keep its standard form Eq. (2) (which is an imperfection of the analogy). Throughout this study, we will assume $c = \text{constant}$, which corresponds to $V = \text{constant} \equiv 0$, but it is valuable to have in mind that the formalism works also in cases where $c^2(\mathbf{r})$ is a slowly varying function of space.

The space differential operators of Eqs. (1) and (2) are identical, and upon separating off the time dependence $\exp(-\mathrm{i}\omega t)$ the resulting amplitude (Helmholtz) equations are the same,

$$\nabla^2\Psi + k_m^2\Psi = 0, \tag{3}$$

$$\nabla^2 p + k^2 p = 0, \tag{4}$$

whereas the difference in their temporal parts leads merely to different dispersion relations between the magnitudes of the wave vectors (k_m, k) and ω, $k_m^2(\mathbf{r}) = (2m/\hbar^2)[\hbar\omega - V(\mathbf{r})]$ and $k^2(\mathbf{r}) = \omega^2/c^2(\mathbf{r})$, which are inputs to the propagator formalism, anyhow. Alternatively, one can also view this in light of the analogy between the quantum mass particle and the phonon. The formalism of the semiclassical propagator, which represents an approximation for the GF of the wave equation, has been thoroughly worked out in the theory of quantum mechanics. According to the above analogy, these results can be directly translated (also) to acoustics.

A. The semiclassical propagator

The time evolution of a dynamical system defines a trajectory $\mathbf{q}(t)$ in phase space, which is the solution of the equations of motion for the initial $\mathbf{q}(t') \equiv \mathbf{q}'$ and final $\mathbf{q}(t'') \equiv \mathbf{q}''$ state of the system. The trajectories are essentially different for a classical and a quantum system. In quantum mechanics an infinite number of trajectories exists that differ in the probability of their occurrence. In contrast, the trajectories in classical mechanics are limited to the one following the deterministic equations of motion.

The transition from quantum to classical behavior is the main subject of the semiclassical theory. In the acoustic context, a trajectory in classical mechanics corresponds to the path of a sound ray—the concept of rays is well-known not only in geometrical optics but also in geometrical acoustics.[25]

Moreover, the semiclassical approximation in mechanics corresponds to the eikonal approximation in optics.

The quantum mechanical propagator describes the time evolution of a quantum wave packet starting out as a delta-function in phase space.[26] In the context of acoustics, the phase space of a single sound ray consists of the position on the ray and its wave vector. For a wave packet initially located at $\mathbf{q}'$ and arriving at $\mathbf{q}''$ after a time t, the semiclassical propagator $K_c(\mathbf{q}'', \mathbf{q}', t)$ can be written using the Van-Vleck equation[22] as

$$K_c(\mathbf{q}'', \mathbf{q}', t) = \sum_{\text{paths}} (2\pi i\hbar)^{-n/2} \exp\left(\frac{i\pi}{4}\right) \sqrt{|C(\mathbf{q}'', \mathbf{q}', t)|} \times \exp\left[\frac{i}{\hbar} S(\mathbf{q}'', \mathbf{q}', t) - i\phi\right]. \tag{5}$$

The summation in Eq. (5) runs over all possible trajectories between the points $\mathbf{q}'$ and $\mathbf{q}''$ of the phase space. Such trajectories are designated as *paths* and are discussed in Sec. II C for the specific implementation. $S(\mathbf{q}'', \mathbf{q}', t)$ is the classical action that fully defines a trajectory and n is the number of space dimensions [$n = 3$ in three dimensions (3D)]. The factor $C(\mathbf{q}'', \mathbf{q}', t)$ represents the density of paths depending on the dimensionality of space and the focusing and defocusing effects of the boundaries. The influence of C for the particular implementation is discussed in Sec. II D. The phase ϕ is a multiple of $\pi/2$, representing the number of conjugate points. These are crossing points of the original trajectory and its infinitesimal perturbation obtained by infinitesimally displacing the initial point $\mathbf{q}'$ (Fig. 1). As conjugate points do not exist in free field or if the room boundaries are flat, they do not appear in the present study and ϕ will be omitted.

B. The GF of the wave equation

The frequency domain representation of the propagator, Eq. (5), is the GF,[22] which is a function of energy E rather than time

$$G(\mathbf{q}'', \mathbf{q}', E) = \sum_{\text{paths}} \frac{2\pi}{(2\pi i\hbar)^{(n+1)/2}} \sqrt{|D(\mathbf{q}'', \mathbf{q}', E)|} \times \exp\left[\frac{i}{\hbar} W(\mathbf{q}'', \mathbf{q}', E)\right], \tag{6}$$

where $D(\mathbf{q}'', \mathbf{q}', E)$ again represents the density of the trajectories and W is the Hamiltonian characteristic function

$$W(\mathbf{q}'', \mathbf{q}', E) = S + Et = \int \mathbf{p} \cdot d\mathbf{s}, \tag{7}$$

with generalized coordinates $\mathbf{s}$ and the associated momenta $\mathbf{p}$.

The GF, Eq. (6), is our starting point and will be now rewritten for the acoustic case, having already in mind its subsequent numerical construction. Let $\mathbf{r}_0$ be the sound source location, $\mathbf{r}$ the observation location, $\mathbf{k}$ the wave vector, and d the length of an individual path $\mathbf{s}(t)$, i.e., the distance the sound particle (phonon)[27] with momentum $\mathbf{p} = \hbar\mathbf{k}$ traveled between $\mathbf{r}_0$ and $\mathbf{r}$. The Hamiltonian characteristic function, Eq. (7), is then $W = \hbar kd$ and, hence, in the acoustic language the GF reads

$$G(\mathbf{r}, \mathbf{r}_0, k) = A \sum_{\text{paths}} B\sqrt{\rho} \exp\left[i\left(kd + \frac{\pi}{4}\right)\right]. \tag{8}$$

The remaining quantities introduced in Eq. (8) are

- A is a normalization factor. As it depends also on technical simulation parameters, it will be determined by calibration (Sec. II F) using the exact analytic solution of the GF in free space.
- Factor B, not present in Eq. (6), is introduced to model the change of the sound ray amplitude when reflecting from the boundary. The value of B changes on each reflection and is in general a $\mathbf{k}$-dependent complex quantity with its absolute value smaller than 1.
- ρ represents the density of the trajectories, analogous to D in Eq. (6), and will be discussed in Sec. II D.

C. Defining the paths

The geometry of the simulation is a rectangular room bounded with weakly absorbing walls (see Sec. II E). Inside the room an omnidirectional (isotropic) sound source is defined as a point located at $\mathbf{r}_0$.

A selected number N of sound rays is emitted from the source in random directions with a uniform solid angle distribution. The sound rays propagate in straight lines and specularly reflect from the room boundaries. The number of reflections M of each ray is a parameter of the simulation.

The sound field is detected in a spherical *observation region* defined by the position of its center $\mathbf{r}$ and the radius R. All sound rays that pass through the observation region are treated as *paths* and are included in the summation of Eq. (8). Importantly, due to the detection in the observation

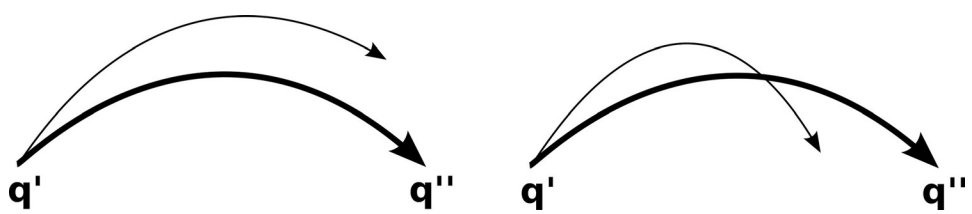

FIG. 1. A graphical representation of a conjugate point: the line in bold represents the original trajectory, while the thin line represents a perturbed trajectory created if the initial point in the phase space $\mathbf{q}'$ is infinitesimally displaced. On the left, the so obtained trajectory does not cross the original one, meaning that no conjugate points exist. On the right, one crossing occurs and one conjugate point is produced.

region of finite size rather than in a point, the GF, Eq. (8), has to be normalized by the density ρ and, hence, becomes

$$G(\mathbf{r},\mathbf{r}_0,k) = A\sum_{\text{paths}} B\sqrt{\frac{1}{\rho}}\exp\left[i\left(kd+\frac{\pi}{4}\right)\right]. \tag{9}$$

The finite size of the observation region limits the spatial resolution of the simulation at high frequencies, where the size of the observation region becomes comparable with the wavelength and, consequently, coarse-graining effects take place. In the present study we focus on the lowest eigenmodes of the room, so this effect is easily avoided.

D. The density of sound rays

The factor ρ in Eq. (8) represents the flux density decrease due to the spreading of sound rays in space, as well as possible focusing/defocusing effects dictated by the boundaries. In the case of flat or piecewise flat boundaries, (de)focusing is absent and, thus, $\rho \propto 1/d^2$ in 3D and $\rho \propto 1/d$ in two dimensions (2D), where d is the total length of the path from $\mathbf{r}_0$ to $\mathbf{r}$, including the reflections. In our 3D simulations, we define

$$\rho \equiv \frac{1}{d^2}. \tag{10}$$

Owing to the overall calibration to be performed in Sec. II F, the proportionality factor is irrelevant. It is, however, important that the same definition, Eq. (10), is used in all cases, regardless of the actual solid angle the source is emitting into. In applications, a possible directionality of a real sound source is then simulated simply by choosing a nonisotropic directional distribution of emitted rays, while the calibration has been fixed once for all.

If the boundaries are curved, in contrast, (de)focusing takes place and no such general relation exists. Although one can numerically compute $\rho(d)$ rather efficiently in this case as well, in the scope of the present study we will not pursue the effects of curved boundaries.

E. The boundary condition

The boundaries are assumed to be locally reacting,[28] meaning that the specular reflection coefficient r (Ref. 29) follows from the local boundary condition, Eq. (27), and depends only on the angle of incidence θ and the ratio $\beta = z_0/z_n$ of specific impedances of air $z_0 = \rho_0 c_0$, with ρ_0 the density of air and c_0 the speed of sound in air, and the wall z_n

$$r = \frac{\cos\theta - \beta}{\cos\theta + \beta}. \tag{11}$$

The absorption coefficient is $\alpha(\theta) = 1 - |r|^2$ and its half-space solid angle average[30] (relevant for the diffuse sound field) is $\bar{\alpha} = 4\beta[\ln(1+\beta^{-1}) - (1+\beta)^{-1}]$ for β real. If $|\beta| \to 0$ (hard wall) or $|\beta| \to \infty$ (soft wall) or $\mathrm{Re}(\beta) = 0$ (lossless wall), then $|r| = 1$ and the reflections conserve acoustic energy. In this study we will use $\beta = 1/60$, corresponding to weak damping with $\alpha(0) = 0.0645$ and $\bar{\alpha} = 0.208$.

As each sound ray is multiply reflected, its amplitude after the ith reflection B is calculated recursively as

$$B_i = rB_{i-1}, \tag{12}$$

with $B_0 = 1$. The efficiency of the method is not compromised if z_n and r depend also on k and not only on θ.

F. Normalization of the GF

The numerical GF, Eq. (9), is calibrated by comparing the result in free space computed according to the prescription of Eq. (9), with the analytical free space solution, in 3D[28]

$$G(\mathbf{r},\mathbf{r}_0,k) = \frac{1}{4\pi d}\exp(ikd). \tag{13}$$

The simulation setup for the free field computation is schematically depicted in Fig. 2. In the absence of boundaries, the path length is simply the geometric distance between the source and the observation region, $d = |\mathbf{r} - \mathbf{r}_0|$, while $B = 1$ as there is no reflection. The normalization factor A of Eq. (9) depends on the simulation parameters in the following manner.

In case of isotropic emission of N rays from the point source, the average number of rays passing through the observation region, if $R \ll d$, is

$$N_1 = \frac{\pi R^2}{4\pi d^2}N, \tag{14}$$

which must be also the result of the numerical summation in Eq. (9), provided that N is large. Hence, using Eqs. (14) and (10), we get

$$G(\mathbf{r},\mathbf{r}_0,k) = A N_1 d\,\exp\left[i\left(kd+\frac{\pi}{4}\right)\right]. \tag{15}$$

By comparison of Eqs. (13) and (15), the normalization factor in the limit $R \ll d$ is

$$A = \frac{1}{\pi R^2 N}\,\exp\left(-i\frac{\pi}{4}\right). \tag{16}$$

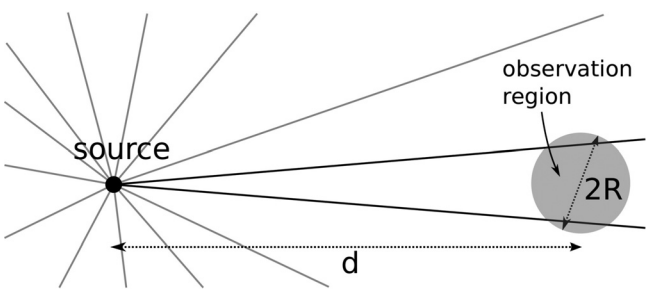

FIG. 2. Sound rays emitted by the point source. Two of them are drawn passing through the observation region (grey area).

Thus, generally, the numerically computed GF needs to be normalized with the factor A, Eq. (16), that depends on the radius of the observation region R and the total number of emitted rays N.

III. ANALYTICAL GF

In this section, analytic results for the GF of the scalar Helmholtz equation, Eq. (4), for the acoustic pressure field $p(\mathbf{r},\omega)$ [where $p(\mathbf{r},t) = p(\mathbf{r},\omega)\exp(-i\omega t)$ and $\omega = kc_0$] in a rectangular room are reviewed. We present an approximation for the GF valid in the limit of weak damping. In our case the damping will take place at the boundaries, which will be assumed weakly absorbing. The analytic result will serve as the basis of comparison for our numerically constructed GF, Eq. (9). A reader not interested in the construction of these analytic representations may safely skip it and jump directly to the last paragraph of Sec. III.

A. GF for the undamped room

The GF of the Helmholtz equation, Eq. (4), satisfying

$$-(\nabla^2 + k^2)G(\mathbf{r},\mathbf{r}_0,k) = \delta(\mathbf{r}-\mathbf{r}_0), \tag{17}$$

is expressed in terms of orthonormal eigenfunctions $\psi_{\mathbf{n}}(\mathbf{r})$ with eigenvalues $k_{\mathbf{n}}^2$,

$$(\nabla^2 + k_{\mathbf{n}}^2)\psi_{\mathbf{n}} = 0, \tag{18}$$

as (cf. e.g., Ref. 31)

$$G(\mathbf{r},\mathbf{r}_0,k) = \sum_{\mathbf{n}} \frac{\psi_{\mathbf{n}}^*(\mathbf{r}_0)\psi_{\mathbf{n}}(\mathbf{r})}{k_{\mathbf{n}}^2 - k^2}. \tag{19}$$

The GF $G_p(\mathbf{r},\mathbf{r}_0,k)$ for physical sound pressure satisfies Eq. (17) with the source (the right-hand side) multiplied by a factor $(\dot{\phi}_m)_0$, representing the amplitude of the rate of change of the radiative mass flux, i.e., the radiative mass acceleration generated by the sound source,

$$-(\nabla^2 + k^2)G_p(\mathbf{r},\mathbf{r}_0,k) = (\dot{\phi}_m)_0\,\delta(\mathbf{r}-\mathbf{r}_0). \tag{20}$$

A constant, frequency-independent $(\dot{\phi}_m)_0$ corresponds to a constant emitted acoustic power P,

$$(\dot{\phi}_m)_0 = \sqrt{8\pi\rho c_0 P}, \tag{21}$$

and with that the pressure GF is

$$G_p(\mathbf{r},\mathbf{r}_0,k) \equiv \sqrt{8\pi\rho c_0 P}\,G(\mathbf{r},\mathbf{r}_0,k). \tag{22}$$

At a perfectly rigid wall with the surface normal $\mathbf{m}$, the equation of motion

$$-i\omega\rho_0\mathbf{v} = -\nabla p, \tag{23}$$

where $\mathbf{v}(\mathbf{r},\omega)$ is the velocity field of air oscillation, requires $\mathbf{m}\cdot\nabla p = 0$. Hence, for a rectangular room defined by $(0,0,0) \le (x,y,z) \le (l_x,l_y,l_z)$, the normalized pressure eigenfunctions are

$$\psi_{\mathbf{n}}(\mathbf{r}) = \frac{1}{\sqrt{C_xC_yC_z}}\cos(k_x x)\cos(k_y y)\cos(k_z z), \tag{24}$$

where $\mathbf{n} = (n_x,n_y,n_z)$, $k_i = \pi n_i/l_i$, $C_i = l_i$ or $C_i = l_i/2$ for $n_i = 0$ or $n_i > 0$, respectively, and $k_{\mathbf{n}}^2 = k_x^2 + k_y^2 + k_z^2 = (\omega_{\mathbf{n}}/c_0)^2$.

B. Weakly damped room

Damping will be included as a perturbation. Due to the absorbing boundary conditions the perturbed operator is non-Hermitian, which implies that the perturbed eigenfunctions are no longer mutually orthogonal and, hence, the expression for the GF, Eq. (19), is no longer exact in principle (see below). The Helmholtz equation, Eq. (4), however, remains unaltered. Therefore, the eigenfunctions are still harmonic. In the ansatz for the perturbed eigenfunction

$$\psi'_{\mathbf{n}}(\mathbf{r}) = X(x)\,Y(y)\,Z(z) \tag{25}$$

with the corresponding perturbed eigenvalues $k'^2_{\mathbf{n}}$, it is convenient to switch to the complex notation,

$$X(x) = Ae^{ik'_x x} + Be^{-ik'_x x}. \tag{26}$$

We need to consider only the function of one coordinate at a time; the other two are then treated separately in an analogous manner.

The boundary condition that corresponds to the one imposed in numerics, Eq. (11), according to Eq. (23) requires on all boundaries

$$\mathbf{m}\cdot\nabla p + i\beta k'_{\mathbf{n}}\,p\,|_{\partial} = 0, \tag{27}$$

with the surface normal $\mathbf{m}$ pointing toward the interior of the room and p proportional to the perturbed eigenfunction, Eq. (25). Consequently,

$$\pm\frac{\partial X}{\partial x} + i\beta k'_{\mathbf{n}}\,X\,|_{\partial_x} = 0 \tag{28}$$

must be fulfilled by the Ansatz, Eq. (26), at $x = 0$ (+) and $x = l_x$ (–). We note that also the constant eigenfunction ($n_x = 0$) gets perturbed as soon as the solution depends on the other coordinates, corresponding to deflections of the wall transverse to the standing wave, that exist when $\beta \neq 0$.

We will assume that β is real. Putting $k'_x = k_x + \delta k_x$ and solving the resulting secular equation to the lowest order of $\beta k_{\mathbf{n}}$ and δk_x, we get

$$n_x > 0: \quad \delta k_x = -\mathrm{i}\frac{2\beta k_{\mathbf{n}}}{\pi n_x}, \tag{29}$$

$$n_x = 0: \quad \delta k_x^2 = -\mathrm{i}\frac{2\beta k_{\mathbf{n}}}{l_x}, \tag{30}$$

which for $n_x > 0$ is a purely imaginary correction to k_x, depending on n_x and through $k_{\mathbf{n}}$ also on n_y and n_z. For $n_x = 0$, the correction $\delta k_x \propto \sqrt{\beta k_{\mathbf{n}}}$ is of lower order, such that the denominator of Eq. (33) gets leading order corrections $k'^2_x = (k_x + \delta k_x)^2$ linear in $\beta k_{\mathbf{n}}$ for all n_x. For $n_x = 0$ and

$k_{\mathbf{n}} = 0$, i.e., for the static mode $\mathbf{n} = (0,0,0)$, the correction $\delta k_x^2 \propto -\beta^2$ is real and of higher order. It slightly displaces the $k \to 0$ singularity of the GF in the negative k direction and can be safely neglected for our purpose. Analogous results hold for δk_y and δk_z.

For completeness, we furnish also the eigenfunction perturbed to the lowest order of $\beta k_{\mathbf{n}}$

$$n_x > 0 : X(x) \propto \cos(k_x x) + \frac{\beta k_{\mathbf{n}}}{k_x l_x}\left[x\,\mathrm{e}^{ik_x x} + (l_x - x)\,\mathrm{e}^{-ik_x x}\right], \tag{31}$$

$$n_x = 0 : \quad X(x) \propto 1 - \mathrm{i}\beta k_{\mathbf{n}}(1 + x/l_x)x \tag{32}$$

and analogously for $Y(y)$ and $Z(z)$.

As a word of general caution and correctness, due to the nonorthogonality of the set $\psi'_{\mathbf{n}}(\mathbf{r})$, in order to obtain the GF for the non-Hermitian operator, one should solve also the adjoint problem (in our case, this is the problem with adjoint boundary conditions) and express the GF with the help of the eigenfunctions of the adjoint operator.[32] However, as the non-Hermitian part of our operator is introduced only by the weak damping perturbation, we will avoid this intricacy and approximate the GF in the usual manner as given by Eq. (19),

$$G'(\mathbf{r}, \mathbf{r}_0, k) = \sum_{\mathbf{n}} \frac{\psi^*_{\mathbf{n}}(\mathbf{r}_0)\psi_{\mathbf{n}}(\mathbf{r})}{k'^2_{\mathbf{n}} - k^2}, \tag{33}$$

where $k'^2_{\mathbf{n}} = k'^2_x + k'^2_y + k'^2_z$ are the perturbed, complex eigenvalues, while $\psi_{\mathbf{n}}(\mathbf{r})$ are the unperturbed eigenfunctions, Eq. (24). With the help of the perturbed eigenfunctions, Eqs. (31) and (32), one can assess the order of magnitude of contributions due to the nonorthogonality.

Moreover, we have compared the analytical GF, Eq. (33), to the direct solution of the wave equation (using the PDE FEM solver COMSOL) with a source of constant acoustic power as specified in Eq. (21). Thereby we verified that for the considered strength of damping, $\beta = 1/60$, the effect of the non-Hermiticity is marginal and Eq. (33) can be considered exact for the purpose: the discrepancy between the two solutions is on the order of $\sim$1%.

IV. RESULTS AND DISCUSSION

To avoid accidental degeneration of the eigenmodes, the numerically investigated rectangular room is chosen to have irrational lengths of the edges, $a \times b \times c = \pi l_0 \times \exp(1) l_0 \times \sqrt{5} l_0$, where l_0 is an arbitrary length defining the length unit. In these units, the lowest resonance of the room, thus, occurs at $k = 1$.

The walls are uniform and weakly absorbing, with the ratio of air and wall impedances $\beta = 1/60$, giving rise to a diffuse field absorption coefficient of $\bar{\alpha} = 0.208$. This value represents a suitable compromise between getting prominent resonances demanded for detailed verification of the method and requiring a modest number ($\sim$100) of reflections per sound ray.

In the presentation of the results, we focus on two aspects. First, the room modes are qualitatively identified by plotting the spatial dependence of the numerically constructed GF at frequencies corresponding to the resonances of the room. Subsequently, the numerical GF is compared with the analytic expression, Eq. (33), in detail.

A. Identification of room modes

The number of emitted sound rays is $N = 180\,000$. The radius of the observation region is $R = 0.095a$. Rather than fixing the number of reflections of each ray, we introduce a low-amplitude cutoff: a ray is terminated when $|B_i| < 2 \times 10^{-4}$. For the chosen geometry and damping strength this gives typically between 100 and 140 reflections per sound ray. The simulation using those parameters runs $\sim$1 h on a single core processor of a desktop computer (no code optimization). In practice, the code was parallelized reducing the computation time accordingly.

The room is divided into a regular cubic mesh of $10 \times 9 \times 7 = 630$ simulation points. The simulation is run for every mesh point that serves both as the sound source and the center of the observation region at the same time, $\mathbf{r} = \mathbf{r}_0$. In all mesh points $G(\mathbf{r}, \mathbf{r}, k)$ is computed according to Eq. (9) for all k values of interest. For every k, the absolute values $|G(\mathbf{r}, \mathbf{r}, k)|$ are averaged into a single quantity designated as the *room GF*, RGF(k). The RGF does not have a direct physical significance, but is a suitable indicator of room resonances in the general case, when the shapes of the room modes are not known *a priori*.

The computed RGF(k) is presented in Fig. 3, showing that the resonance peaks coincide well with the analytic eigenfrequencies of the undamped rectangular room. This means that the method can be used to predict room resonances in practice. The increase of the RGF for $k \to 0$ represents the response of the room to nearly static compression, which is acoustically not relevant.

For the lowest six resonances, $|G(\mathbf{r}, \mathbf{r}, k)|$ in all mesh points is shown in Fig. 4, which thus represents the shapes of the room pressure modes. The results show qualitative agreement with the eigenfunctions, Eq. (24). It can be clearly seen that the three lowest modes are axial, with the highest

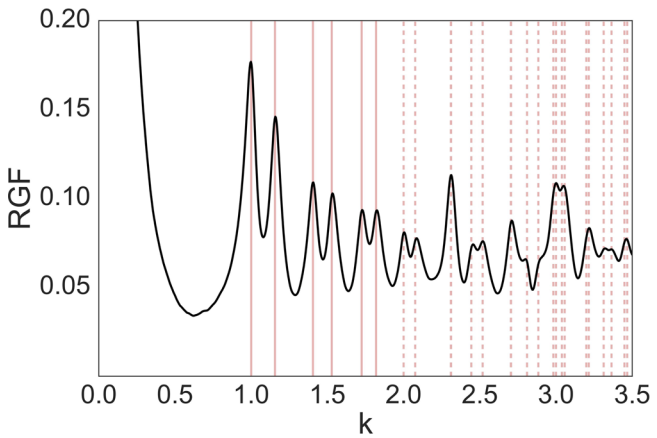

FIG. 3. (Color online) The numerical RGF(k) and analytic k values of the resonances for the undamped rectangular room (vertical lines). Six lowest resonances are indicated as solid vertical lines, for which the corresponding room modes are presented in Fig. 4. The frequency $f = kc_0/(2\pi l_0)$ is inversely proportional to the length scale l_0 of the room.

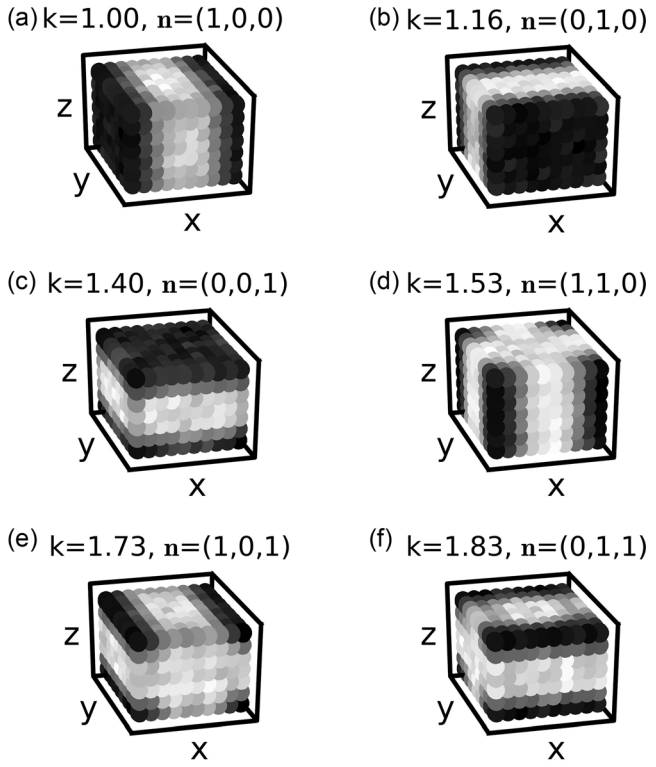

FIG. 4. Numerical $|G(\mathbf{r},\mathbf{r},k)|$, acquired in detection spheres centered at the mesh points; large values are drawn dark. The values of k correspond to the peaks of RGF(k) in Fig. 3.

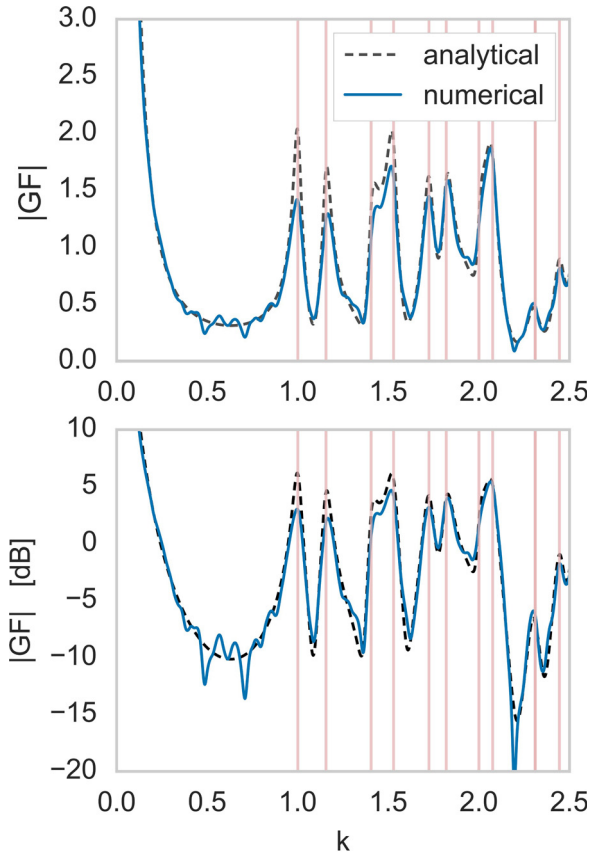

FIG. 5. (Color online) The numerical |GF| (solid curve) and the analytic formula, Eq. (33) (dashed); the lower graph is in dB scale with the reference value of 1. The solid vertical lines correspond to the undamped resonances. The frequency $f = kc_0/(2\pi l_0)$ is inversely proportional to the length scale l_0 of the room.

pressure occurring at parallel walls. In contrast, the higher three modes that are presented are "tangential," which are a combination of two axial modes so that the pressure maxima occur at parallel edges.

It can be also seen that the nodes of the modes occur at proper positions and that the gradual pressure change in between the extremes of the pressure is modeled correctly notwithstanding some evident numerical error.

B. Numerical GF

The number of emitted sound rays is $N = 2\,160\,000$. Without parallelization, this simulation would run ∼20 h on a single core processor of a desktop computer (no code optimization). The radius of the observation region is $R = 0.048a$. The sound source and the observation region are positioned in diagonally opposite room corners $0.095a$ away from each wall. The absolute value of the numerical GF, $|G(\mathbf{r},\mathbf{r}_0,k)|$, is presented in Fig. 5, where it is compared to the GF, Eq. (33), at the same $\mathbf{r}$ and $\mathbf{r}_0$. From this rigorous and quite selective test of the numerical method we can conclude the following:

- The numerical and the analytic solutions are generally consistent.
- The position of the peaks of the numerical |GF| coincide with the resonances.
- For $k < 1$, the numerical |GF| precisely follows the analytic dependence.
- The absolute widths of the numerical and analytic resonances match. In contrast, the peaks of |GF| are underestimated, in particular, at the lowest modes. This is inherently attributed to the semiclassical (eikonal) approximation and will be a subject of further research.
- Some numerical noise can be observed at lower values of |GF|.

V. CONCLUSION

An advanced geometric ray-tracing numerical method based on the semiclassical (eikonal) approximation was used to model the GF of the scalar wave equation in a cuboid room. The underlying theory was reviewed and all important aspects of the numerical implementation were presented. For the purpose of rigor, as well as to facilitate the comparison with analytic results, the computational method was used in the regime of weak damping, resulting in distinct and pronounced resonance peaks.

As an indicator of the acoustic resonances, the room GF, RGF(k), was computed, showing well-defined peaks at the resonance frequencies of the room. Furthermore, the corresponding pressure modes show a convincing qualitative agreement with the expected eigenfunctions of the cuboid room. It follows that the presented geometric ray-tracing method can be potentially used to identify the modes of the room, unless its shape is very specific. Moreover, a systematic agreement between the numerically constructed GF and its analytic formula was demonstrated. As the GF represents the full solution of the wave equation, this is a severe test and passing it is a substantial

result. Further studies are to be conducted to characterize the performance of the method in a wider set of circumstances.

It is important to bear in mind that at higher frequencies the modal overlap increases and, consequently, the modeling of individual modes has no advantage for the numerical determination of room acoustic parameters. In fact, in the high frequency region bare geometrical methods are broadly used, meaning that modeling issues at higher k values are far less severe from a strictly acoustical perspective.

One must be aware that although the method correctly identifies the modes of the investigated cuboid room, this does not automatically mean that it produces equally reliable results for any room geometry, as it—like any geometric method—disregards diffraction, the importance of which depends on the type of geometry. Generally, in star-convex room geometries diffraction contributions are less significant and we can expect physically meaningful results also in those general cases. However, if geometric shadow zones are present in the room, diffraction can be dominant in these zones (its relative importance depends also on the portion of the rays arriving there via reflections) and the use of geometrical acoustics is not adequate. Efforts to overcome this limitation, at least to a certain extent, are a part of our ongoing investigations.

In conclusion, the presented advanced geometric modeling technique appears as a promising candidate in low-frequency acoustic modeling, which is conventionally not within the effective range of geometric modeling. In perspective, supported by the findings of this proof-of-concept study, future research should branch into three main directions: (1) reliability and fundamental accuracy issues in the rectangular geometry (advantage: no diffraction errors), (2) validation and characterization of the method for general room geometries (including (de-)focusing effects in case of curved boundaries) and various boundary conditions that appear in practice, and (3) attempts to include diffraction. One should not disregard the importance of point (1): as already mentioned in the Introduction and confirmed also in Sec. IV B, geometrical methods bear a class of problems that are not related to diffraction. These can be best addressed in the rectangular geometry, where they are not blurred by diffraction errors. The more technical aspects include addressing the issues of computational complexity and optimization, as ray tracing largely benefits from parallelization.

ACKNOWLEDGMENTS

The authors acknowledge partial support of the Slovenian Research Agency (Grant Nos. N1-0019, J1-7435), the Slovenian Ministry of Higher Education, Science and Technology, and the European Regional Development Fund.

[1]Y. Kawai, "Boundary element method for computing transient acoustic waves in a room," Kansai University Report No. 49 (2007), pp. 69–77.
[2]V. Easwaran and A. Craggs, "On further validation and use of the finite-element method to room acoustics," J. Sound Vib. **187**, 195–212 (1995).
[3]K. Kowalczyk and M. van Walstijn, "Virtual room acoustics using finite difference methods. How to model and analyse frequency-dependent boundaries?," in *International Symposium on Communications, Control, and Signal Processing*, St. Julians, Malta (2008), Vol. 187, pp. 1504–1509.
[4]W. Desmet and D. Vandepitte, "Finite element method in acoustics," in *ISAAC 13- International Seminar on Applied Acoustics*, Leuven, Belgium (2002), pp. 37–81.
[5]I. Harari and T. J. R. Hughes, "A cost comparison of boundary element and finite element methods for problems of time-harmonic acoustics," Comput. Methods Appl. Mech. Eng. **97**, 77–102 (1992).
[6]A. Krokstad, S. Strom, and S. Sørsdal, "Calculating the acoustical room response by the use of a ray tracing technique," J. Sound Vib. **8**, 118–125 (1968).
[7]G. Naylor, "ODEON Another hybrid room acoustical model," Appl. Acoust. **38**(2-4), 131–143 (1993).
[8]B.-I. Dalenbäck, "A new model for room acoustic prediction and auralization," Ph.D. thesis, Chalmers University of Technology, Gothenburg, Sweden, 1995.
[9]T. Le Pollès, J. Picaut, S. Colle, M. Bérengier, and C. Bardos, "Sound-field modeling in architectural acoustics by a transport theory: Application to street canyons," Phys. Rev. E **72**, 046609 (2005).
[10]J. Picaut, J. Hardy, and L. Simon, "Sound propagation in urban areas: A periodic disposition of buildings," Phys. Rev. E **60**, 4851–4859 (1999).
[11]J. B. Allen and D. A. Berkley, "Image method for efficiently simulating small-room acoustics," J. Acoust. Soc. Am. **65**, 943–950 (1979).
[12]T. Funkhouser, N. Tsingos, I. Carlbom, G. Elko, G. Pingali, M. Sondhi, J. West, G. Elko, P. Min, and A. Ngan, "A beam tracing method for interactive architectural acoustics," J. Acoust. Soc. Am. **115**, 739–756 (2004).
[13]M. Vorländer, "Simulation of the transient and steady-state sound propagation in rooms using a new combined ray-tracing/image-source algorithm," J. Acoust. Soc. Am. **86**, 172–177 (1989).
[14]M. Vorländer, "Computer simulations in room acoustics: Concepts and uncertainties," J. Acoust. Soc. Am. **133**, 1203–1213 (2013).
[15]L. Savioja and U. P. Svensson, "Overview of geometrical room acoustic modeling techniques," J. Acoust. Soc. Am. **138**, 708–730 (2015).
[16]A. Pompei, M. A. Sumbatyan, and N. F. Todorov, "Computer models in room acoustics: The ray tracing method and the auralization algorithms," Acoust. Phys. **55**, 821–831 (2009).
[17]J. S. Suh and P. A. Nelson, "Measurement of transient response of rooms and comparison with geometrical acoustic models," J. Acoust. Soc. Am. **105**, 2304–2317 (1999).
[18]C.-H. Jeong, I. Jeong-Guon, and J. Rindel, "An approximate treatment of reflection coefficient in the phased beam tracing method for the simulation of enclosed sound fields at medium frequencies," Appl. Acoust. **69**, 601–613 (2008).
[19]S. M. Dance, J. P. Roberts, and B. M. Shield, "Computer prediction of sound distribution in enclosed spaces using an interference pressure model," Appl. Acoust. **44**, 53–65 (1995).
[20]M. Aretz, P. Dietrich, and M. Vorländer, "Application of the mirror source method for low frequency sound prediction in rectangular rooms," Acta Acust. Acust. **100**, 306–319 (2014).
[21]M. Schröder, "Die statistischen parameter der frequenzkurven von grossen räumen" ("Statistical parameters of frequency responses in large rooms"), Acta Acust. Acust. **4**, 594–600 (1954).
[22]M. C. Gutzwiller, *Chaos in Classical and Quantum Mechanics* (Spring, New York, 1990), pp. 186, 188.
[23]R. Bellman and R. Vasudevan, *Wave Propagation—An Invariant Imbedding Approach* (Springer, The Netherlands, 1986), p. 21.
[24]M. Bass, *Handbook of Optics: Volume I—Geometrical and Physical Optics, Polarized Light, Components and Instruments* (McGraw-Hill Professional, 2010).
[25]A. D. Pierce, *Acoustics –An Introduction to Its Physical Principles and Applications* (Acoustical Society of America, Melville, New York, 1989), pp. 371–388.
[26]P. Cvitanović, R. Artuso, R. Mainieri, G. Tanner, and G. Vattay, *Chaos: Classical and Quantum* (Niels Bohr Institute, Copenhagen, 2012), pp. 634–637. Available at ChaosBook.org (Last viewed 21 April 2016).
[27]W. B. Joyce, "Classical-particle description of photons and phonons," Phys. Rev. D **9**, 3234–3256 (1974).
[28]T. D. Rossing, *Springer Handbook of Acoustics* (Springer, New York, 2007), pp. 60, 85.
[29]H. Kuttruff, *Acoustics: An Introduction* (Taylor and Francis, New York, 2007), p. 100.
[30]P. M. Morse and K. Uno Ingard, *Theoretical Acoustics* (McGraw-Hill, New York, 1968), p. 580.
[31]S. Hassani, *Mathematical Physics: A Modern Introduction to Its Foundations* (Springer International Publishing, Switzerland, 2013), p. 630.
[32]P. M. Morse and H. Feshbach, *Methods of Theoretical Physics, Part I* (McGraw-Hill, New York, 1953), p. 886.